Effect of Frequency on Hydrodynamic Parameters of Mesh Fillers in Oscillatory Flow

E.C. Landrum[1], T.J. Conrad[2], M.G. Pathak[2], S.M. Ghiaasiaan[2], C.S.Kirkconnell[3], T. Crittenden[4], S. Yorish[4]

[1]Siemens, Orlando, FL 32801
[2]Georgia Institute of Technology, Atlanta, GA 30332
[3]IRIS Technology, Irvine, CA 92602
[4]Virtual AeroSurface Technologies, Atlanta, GA 30318

ABSTRACT

An experimental investigation was carried out to determine the effect of frequency on the porous media hydrodynamic closure relations for steady periodic flow. Using room temperature helium as the working fluid, stacked discs of #635 stainless steel and #325 phosphor bronze wire meshes were subjected to an oscillatory flow field. Dynamic pressure transducers recorded waveforms upstream and downstream of the porous section at charge pressures of 2.86 and 3.55 MPa. Tests were performed in the axial direction at frequencies ranging from 50 to 200 Hz. Hydrodynamic parameters were determined using a CFD-assisted methodology. The experimental test section and its vicinity were simulated using the Fluent code and mesh fillers were modeled as a porous structure. Model porous media hydrodynamic parameters were iteratively adjusted to match the model predictions to the experimental results. Directional resistances related to the Darcy permeability and Forchheimer's inertial coefficients were obtained at discrete frequencies and errors were quantified. The experimental results indicate that Forchheimer's inertial coefficient may depend rather strongly on frequency. More detailed experiments are needed to ascertain the observed trends.

INTRODUCTION

A number of methods and tools are available for design, analysis and optimization of regenerative cryocooler systems. Accurate modeling requires closure relationships, particularly with respect to the hydrodynamic and thermal transport processes of the micro porous structures which comprise the regenerators and heat exchangers. Hydrodynamic resistances of these porous components can have a profound effect on system performance as pressure drop and phase shift across the regenerator, as well as the heat exchangers, is vital to cooling efficiency. Experimental data and correlations have been published for some widely used filler materials suitable for large and small scale devices[1-4]. Research has suggested that hydrodynamic parameters may be a function of charge pressure, temperature, flow regime and frequency of oscillation[2-6]. Much of these phenomena are not well understood and measurement of hydrodynamic resistances remains specific to a particular application and range of experimental conditions.

Cryocoolers 16, edited by S.D. Miller and R.G. Ross, Jr.

Some investigations have shown that directional oscillatory flow parameters can be different from those determined for steady flow. Hsu[7,8] has suggested that parameters determined for low frequency oscillation limited to 4 Hz mimic results obtained for steady flow. In this sense, the oscillatory resistance parameters are regarded as quasi-steady. Other studies indicate significant discrepancies between resistances determined for oscillating flow conditions and those obtained under steady flow[2-4]. The data often exhibit an increased resistance for oscillatory flows. Several correlations have been proposed to capture the effect of frequency on hydrodynamic resistances[5,6], however, results are widespread and inconsistent.

This investigation seeks to determine the effect of frequency on the hydrodynamic parameters of stacked discs of #325 phosphor bronze and #635 stainless steel wire screens. Experiments were performed in the axial direction at fill pressures of 2.86 and 3.55 MPa. Pressure waveforms at the inlet and outlet of the porous samples were obtained at discrete operating frequencies ranging from 50 to 200 Hz. By simulating the experimental setup and its vicinity using CFD, sample resistance parameters were iteratively adjusted until simulated predictions matched experimental results. This method of formulating hydrodynamic characteristics originated from numerical methods developed by Harvey[1]. Cha[2] further developed this process through the incorporation of CFD analysis.

EXPERIMENTAL METHODS

Wire cloth material was supplied by TWP Inc. (Berkeley, Ca) and test samples were machined by Virtual AeroSurface Technologies (Atlanta, Ga) using a punching operation. Both samples possess a plain square weave pattern and are characterized by the numbers of parallel strands of wires per inch within the mesh matrix. A random orientation and uniform packing density were adopted during packing of the screens in order to imitate industry standards. The intrinsic properties of the investigated porous materials, including pore size, wire diameter and porosity, are summarized in Table 1. Sample porosities were calculated using the occupied volume of the specimen housing, aggregate sample mass and an average material density.

The experimental setup included a tactical compressor (Hughes Aircraft Company), function generator (HP-Agilent 33120A), data acquisition control unit (HP-Agilent 3852A), amplifier (Crown DC-300A series II), two high frequency dynamic pressure transducers (PCB Piezotronics 101A05) and the test section containing the porous sample. The dynamic pressure sensors have a resolution of 0.014 kPa. An HP VEE virtual console was used to integrate all sensor measurements and store the output data. An iron core transformer was also utilized to offer better power transmission from the amplifier to the compressor. A schematic of the oscillatory axial flow test setup is shown in Figure 1.

The oscillatory flow experimental setup is a closed system bounded by the compressor and valve V1, and employs ultra high purity helium as the working fluid. All testing was conducted at ambient temperatures of approximately 300 K. Before testing, the apparatus was purged of air and contaminants, and test runs were only performed after strict assurance of a hermetically sealed setup.

The axial flow test section which houses the porous media is a hollow aluminum cylinder with two inner diameters separated by a step change. A 2.0 mm passage opens up to a 4.013 mm diameter channel which contains the stacked screens. End pieces bolted onto flanges located on either side of the test section constrain the axial sample and provide mounts for sensory equipment. The test sample and housing were designed with a large aspect ratio of 3.2 to ensure that the flow within the porous structure is predominately axial. Strict tolerance used in fabrication ensured a negligible clearance between the stacked screens and the test section's inner diameter.

During each test, pressure sensors located on the inlet and outlet of the porous test section sampled periodic pressure waveforms and the virtual console represented these signals by their

Table 1: Test sample details

	Sample Geometry		Mesh Geometry			Measured
Porous Media	Dia [mm]	Length [mm]	Wire Dia [micron]	Pore Size [micron]	Thickness [micron]	Porosity [-]
#325 Phosphor Bronze	4.0	12.7	35.6	43	43	0.6738
#635 Stainless Steel	4.0	12.7	20.3	20	25	0.6163

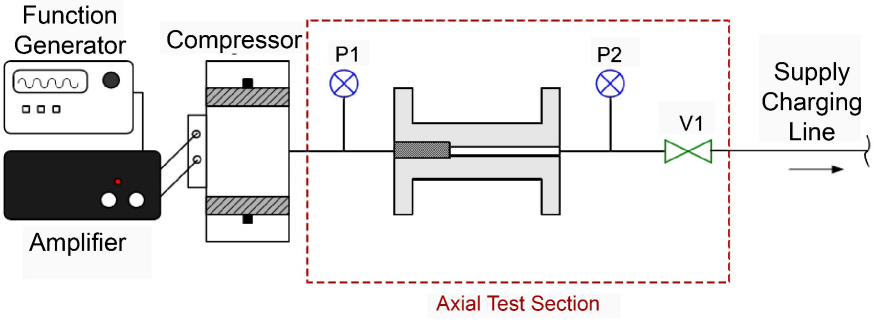

Figure 1: Experimental Setup

first three harmonics using a Fast Fourier Transform (FFT). This representation of the signal is shown in Eqn. 1, where pressure amplitudes are expressed as Z_j and the phase angles are represented with ϕ_j. The mean pressure, not included in this representation, was set as the operating pressure for the CFD analysis and the pressure waveform recorded at P1 was applied as an inlet boundary condition.

$$P_{osc} = Z_1 \cos\left(\omega t + \phi_1\right) + Z_2 \cos\left(2\omega t + \phi_2\right) + Z_3 \cos\left(3\omega t + \phi_3\right) \tag{1}$$

High and low flow data was taken for each sample at seven distinct frequencies in the 50 to 200 Hz range, in 25 Hz intervals, at charge pressures of 2.86 and 3.55 MPa. Low flow data is obtained at a pressure amplitude of about 7 kPa at the P1 location, set by adjusting the compressor input power. High flow data was measured at the largest attainable pressure amplitude for a given frequency, limited by the compressor's frequency response which diminishes with increasing frequency. The electrical power input for the compressor was constrained to about 100 W to prevent damage.

THEORY

Standard conservation equations for mass, momentum and energy can be applied to analyze flow fields in open gas channels. Through the application of volume-averaged conservations equation, standard and workable governing equations are obtained for flow within porous structures. Although this method masks local fluid-solid interaction at the pore level, the macroscopic fluid behavior is captured. The volume-averaged fluid conservation equations for continuity, momentum and energy in porous media are, respectively,

$$\frac{\partial}{\partial t}\left(\varepsilon\rho\right) + \nabla\cdot\left(\varepsilon\rho\vec{v}\right) = 0 \tag{2}$$

$$\frac{\partial}{\partial t}\left(\varepsilon\rho\vec{v}\right) + \nabla\cdot\left(\varepsilon\rho\vec{v}\vec{v}\right) = -\varepsilon\nabla P + \nabla\cdot\left(\varepsilon\bar{\bar{\tau}}\right) + \varepsilon\vec{F}_{bf} - \mu\bar{\bar{D}}\cdot\vec{v} - \frac{\bar{\bar{C}}\rho}{2}\cdot\left|\vec{v}\right|\vec{v} \tag{3}$$

$$\frac{\partial}{\partial t}\left(\varepsilon\rho_f e_f + \left(1-\varepsilon\right)\rho_{sol}e_{sol}\right) + \nabla\cdot\left(\varepsilon\vec{v}\left(\rho_f e_f + P\right)\right) - \nabla\cdot\left(\left(\varepsilon k_f + \left(1-\varepsilon\right)k_{sol}\right)\nabla T + \bar{\bar{\tau}}\cdot\varepsilon\vec{v}\right) = 0 \tag{4}$$

The coefficients of the hydrodynamic loss terms on the right side of the momentum equation can be determined through empirical relations. In the momentum equation ($\bar{\bar{D}}$) stands for the viscous resistance coefficient tensor, while ($\bar{\bar{C}}$) represents the inertial resistance tensor. When applying these parameters to an anisotropic medium using the principle directions of the porous medium, they can be represented by the directional Darcy permeability and Forchheimer's inertial coefficient, where *i* represents each principle coordinate,

$$K_i = \frac{\varepsilon^2}{D_i} \tag{5}$$

$$c_{f_i} = \frac{C_i \sqrt{K_i}}{2\varepsilon^3} \tag{6}$$

This investigation analyzes and determines these parameters separately for each discrete frequency. It should be noted that there are complimentary forms of accounting for hydrodynamic losses such as a friction factor. Correlations for frequency dependent friction factors have been proposed in the past, however, comparison is difficult as there are multiple length scales and Reynold's number representation.

COMPUTATIONAL METHODS

The Fluent CFD package[9] was used to determine the hydrodynamic parameters. CFD cases were created to model the fluid control volume within the test section geometry in Figure 1 between the P1 pressure transducer location and the valve V1. All simulations were two-dimensional, axisymmetric representations of the experimental test section and its vicinity. Nodalized grids were created using the Gambit software and then imported into Fluent. Grid dependence studies were performed on multiple grids for each case to determine how nodal spacing effected output variables. A mesh with the smallest cell count and largest spacing which provided negligible change in the results was employed, affording the most efficient use of computational time. A grid with 6,731 quadrilateral elements was used for all cases.

In all simulations, pure helium was modeled as a Newtonian fluid using the ideal gas equation of state. Open fluid volumes utilized the standard governing equations for laminar flow regimes while fluid behavior within the porous media was governed through volume-averaged conservation equations. For porous regions, the local fluid and solid phases were assumed to be in thermal equilibrium and the appropriate sample porosities are applied. Walls were modeled as smooth adiabatic surfaces and gravitational body forces were not included. Constant viscosity was applied to the fluid as temperatures remained relatively constant. A universal set of convergence criteria restricting residual values to less than 1E-7 were applied to all simulations.

The CFD code utilized input values for a porous zone's viscous and inertial resistances. It was these values which were iteratively adjusted until the simulation's predicted output variables matched the experimental measurements. The viscous and inertial resistances in the radial direction were assumed to be equal to their corresponding axial-direction values when determining the hydrodynamic parameters, since the flow within the porous samples has a predominately axial velocity component and therefore the errors resulting from the inaccuracy of the radial hydrodynamic parameters are small.

Pressure waveforms were experimentally measured for both filler materials at two distinct charge pressures and a range of operating frequencies. Separate high and low flow CFD cases were constructed for each filler material at each frequency and charge pressure. For each case, the corresponding FFT representation of the experimentally measured pressure signal at P1 was applied as a user defined pressure inlet boundary condition at the P1 location. Values for the porous region's viscous and inertial resistances were applied and each simulation was iterated for five periods of pressure oscillations before it was regarded as being at steady-periodic state. This allowed time for any transient phenomena to stabilize.

Monitors recorded the simulation's area-weighted average static pressure at the P1 and P2 locations at each time step. Time steps were chosen for each operating frequency to provide a temporal resolution of at least 1 deg in phase. The simulated pressure at the P2 location was compared to the experimentally measured pressure waveform at the P2 location to determine the oscillatory hydrodynamic parameters. Pressure amplitudes and phase angles, measured with respect to the pressure signal at P1, were compared for the simulated and experimental waveforms at P2 and matched as closely as possible.

Viscous and inertial resistances were first determined using the low and high flow cases, respectively, for each frequency. These parameters were iteratively adjusted for each case until there was good agreement between the simulated and experimental dynamic pressures at the P2 location. At low flow conditions, inertial effects are small and the viscous resistances may be more easily determined; for these cases, the inertial resistance was held constant and the viscous resistance

adjusted. Although the relative contribution of the inertial resistance term on the overall governing equations was small in these cases, approximate values of 50,000 and 40,000 m^{-1} were still applied for the inertial resistances of the #325 phosphor bronze and #635 stainless steel samples, respectively. These approximate values were determined in a previous study[4].

Once the viscous resistances were established, the inertial coefficients were then determined using the higher flow rate cases. In this process, the viscous resistances previously obtained from the corresponding low flow rate cases were applied and held constant and only the inertial resistances were adjusted.

RESULTS

Hydrodynamic parameters were determined for each sample over a range of frequencies at charge pressures of 3.55 and 2.86 MPa. Resolutions of 1.0E-12 and 1.0E-13 m^{-2} were used when solving for the viscous resistances of the #325 phosphor bronze and #635 stainless steel filler materials, respectively. The average errors in pressure amplitude between the simulations and experimental data were 15.8 and 5.9 Pa for the #325 phosphor bronze and stainless steel cases, respectively. The average errors in phase angle for these cases were 0.025 and 0.020 rad, respectively. Results for the frequency dependent Darcy permeability are displayed in Figure 2.

Figures 2(A) and 2(B) indicate that the #325 phosphor bronze sample has a larger permeability than the # 635 stainless steel sample. The data for the #325 phosphor bronze sample indicate a slight filling pressure dependence at frequencies up to about 100 Hz, and little pressure effect for higher frequencies. These data also suggest that permeability decreases with frequency, approaching a constant value for frequencies higher than about 100 Hz. No clear trend in frequency dependence can be deduced from the data representing # 635 stainless steel.

Once the viscous resistances were determined, they were then applied to the high flow cases and held constant as the inertial resistances were evaluated. A resolution of 0.1 was used for both materials when solving for the Forchheimer's coefficients. Errors remained small for the inertial parameterization. Average deviations in pressure amplitude and phase lag of 45.7 Pa and 0.007 rad were reported for the phosphor bronze sample while the stainless steel cases produced average errors of 49.0 Pa and 0.030 rad. Figure 3 shows the frequency dependent inertial coefficients for the two samples.

Although some scatter is present, a decreasing trend is seen with the Forchheimer's inertial coefficients for both the #325 phosphor bronze and #635 stainless steel samples across the range of tested frequencies. Table 2 summarizes the permeability and inertial coefficients for the discrete frequencies and charge pressures.

The results of this investigation are somewhat inconclusive. Weak dependence of parameters on frequency was observed, with the Darcy Permeability for the #325 phosphor bronze and Forchheimer's Coefficient for both materials decreasing with increasing frequency. The Darcy Per-

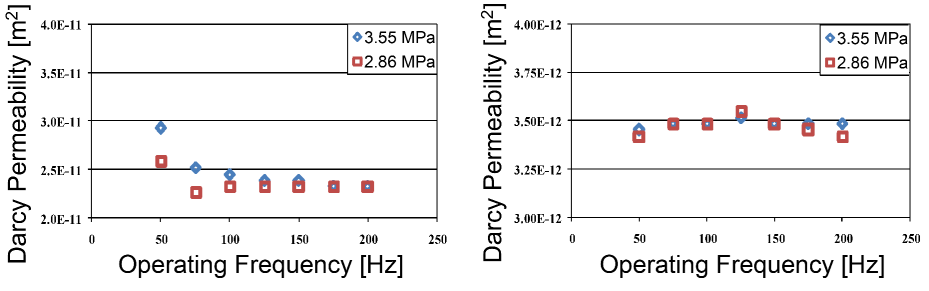

(A) (B)

Figure 2: Frequency dependent Darcy permeabilities for the (A) #325 phosphor bronze (67.38%) and (B) #635 stainless steel (61.63%)

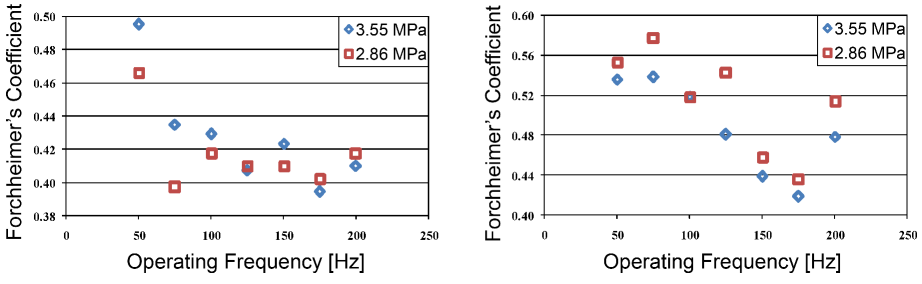

Figure 3: Frequency dependent Forchheimer's inertial coefficient for the (A) #325 phosphor bronze (67.38%) and (B) #635 stainless steel (61.63%)

Table 2: Test sample frequency dependent resistance parameters

Phosphor Bronze #325					Stainless Steel #635				
Charge Pressure [MPa]	Operating Frequency [Hz]	Porosity [-]	Darcy Permeability [m^2]	Forchheimer's Coefficient [-]	Charge Pressure [MPa]	Operating Frequency [Hz]	Porosity [-]	Darcy Permeability [m^2]	Forchheimer's Coefficient [-]
2.86	50	0.6738	2.59E-11	0.4662	2.86	50	0.6163	3.42E-12	0.5531
2.86	75	0.6738	2.27E-11	0.3971	2.86	75	0.6163	3.48E-12	0.5781
2.86	100	0.6738	2.33E-11	0.4180	2.86	100	0.6163	3.48E-12	0.5183
2.86	125	0.6738	2.33E-11	0.4101	2.86	125	0.6163	3.55E-12	0.5433
2.86	150	0.6738	2.33E-11	0.4101	2.86	150	0.6163	3.48E-12	0.4585
2.86	175	0.6738	2.33E-11	0.4022	2.86	175	0.6163	3.45E-12	0.4366
2.86	200	0.6738	2.33E-11	0.4180	2.86	200	0.6163	3.42E-12	0.5136
3.55	50	0.6738	2.93E-11	0.4953	3.55	50	0.6163	3.45E-12	0.5358
3.55	75	0.6738	2.52E-11	0.4350	3.55	75	0.6163	3.48E-12	0.5382
3.55	100	0.6738	2.45E-11	0.4291	3.55	100	0.6163	3.48E-12	0.5183
3.55	125	0.6738	2.39E-11	0.4074	3.55	125	0.6163	3.52E-12	0.4807
3.55	150	0.6738	2.39E-11	0.4234	3.55	150	0.6163	3.48E-12	0.4386
3.55	175	0.6738	2.33E-11	0.3943	3.55	175	0.6163	3.48E-12	0.4186
3.55	200	0.6738	2.33E-11	0.4101	3.55	200	0.6163	3.48E-12	0.4784

meability of the #635 stainless steel first increased and then decreased with increasing frequency, although this may simply be scatter around a mean value. In view of the scatter that existed in the results, the observed trends need further experimental verification.

One experimental issue which may have contributed to the uncertainty in the results was that the pressure amplitudes and resulting oscillatory mass flow rates supplied by the compressor rolled off drastically as the frequency increased. With reduced input pressure amplitude and mass flow, the relative contribution of the inertial resistance term to the overall pressure drop and phase difference varies with frequency, decreasing as the frequency increases. At higher frequencies it is therefore more difficult to determine the inertial resistance with the current experimental apparatus.

It should also be noted that this study was performed over a relatively small range of operating frequencies and charge pressures. A broader range of test frequencies and charge pressures would be needed for future investigations. While higher frequency experiments may be more difficult due to compressor limitations, extending these tests to lower frequencies may prove useful in bridging the gap between steady and oscillatory flow resistance parameters.

CONCLUDING REMARKS

The dependence of oscillatory flow porous media hydrodynamic parameters on frequency was investigated with experiments and CFD modeling. Viscous and inertial resistance parameters were determined for stacked screens of #635 stainless steel and #325 phosphor bronze at discrete operating frequencies in the range of 50 to 200 Hz. Charge pressures of 3.55 and 2.86 MPa were applied. The experimental test setup was simulated using a CFD code and experimental data was applied for the model boundary conditions. In the CFD model, axial hydrodynamic parameters for the sample materials were iteratively adjusted until simulated predictions matched experimental results. Low and high flow experimental data were obtained at each frequency in order to separately determine

the viscous and inertial resistances, respectively. The results are presented as frequency dependent Darcy permeabilities and Forchheimer's inertial coefficients. Relatively clear trends were observed in the Darcy permeability for the #325 phosphor bronze, and for the Forchheimer's inertial coefficients for both materials. However, no clear trend could be identified for the stainless steel sample over the investigated frequency range. Further investigation over a broader range of operating frequencies, particularly lower frequencies, is recommended.

REFERENCES

1. Harvey, J. P., "Oscillatory Compressible Flow and Heat Transfer in Porous Media – Application to Cryocooler Regenerators," Doctoral Thesis, Georgia Institute of Technology, Atlanta, GA (2003).
2. Cha, J.S., "Hydrodynamic Parameters of Micro Porous Media for Steady and Oscillatory Flow: Application to Cryocooler Regenerators," Doctoral Thesis, Georgia Institute of Technology, Atlanta, GA (2007).
3. Clearman, W.M., "Measurement and Correlation of Directional Permeability and Forchheimer's Coefficient of Micro Porous Structures Used in Pulse-Tube Cryocoolers," Masters Thesis, Georgia Institute of Technology, Atlanta, GA (2007).
4. Landrum, E.C., "Anisotropic Parameters of Mesh Fillers Relevant to Miniature Cryocoolers," Masters Thesis, Georgia Institute of Technology, Atlanta, GA (2009).
5. Nam, K., Jeong, S., "Investigation of Oscillating Flow Friction Factor for Cryocooler Regenerator Considering Cryogenic Temperature Effect," *Cryogenics* 45 (2006), pp. 733-738.
6. Shen, Q.Q., Ju, Y.L., "A New Correlation of Friction Factor for Oscillating Flow Regenerator Operating at High Frequencies," AIP Conference Proceedings 985 (2008), pp. 267-274.
7. Hsu, C., Fu, H., Cheng, P., "On Pressure-Velocity Correlation of Steady and Oscillating Flows in Regenerators Made of Wire Screens," *Journal of Fluids Engineering* 121 (1999), pp. 52-56.
8. Hsu, C., *Handbook of Porous Media* (2nd Ed.), Taylor and Francis Group, Boca Raton (2005), pp. 39-64.
9. FLUENT 6.3 Users Manual, Fluent Inc., 2008.